Title: **NEUTRON COINCIDENCE IMAGING FOR ACTIVE AND PASSIVE NEUTRON ASSAYS**

Author(s): Robert J. Estep, Glen Brunson, and Sheila Melton

Submitted to:

http://lib-www.lanl.gov/cgi-bin/getfile?00796673.pdf

NEUTRON COINCIDENCE IMAGING FOR ACTIVE AND PASSIVE NEUTRON ASSAYS

Robert J. Estep, Glen Brunson, and Sheila Melton
Los Alamos National Laboratory
Los Alamos, New Mexico, 87545, USA 505/667-3683

ABSTRACT

Neutron multiplicity assay algorithms for ^{240}Pu assume a point source of fission neutrons that are detected in a single detector channel. The ^{240}Pu in real waste, however, is more likely to be distributed throughout the container in some random way. For different reasons, this leads to significant errors when using either multiplicity or simpler coincidence analyses. Reduction of these errors can be achieved using tomographic imaging. In this talk we report on our results from using neutron singles and coincidence data between tagged detector pairs to provide enhanced tomographic imaging capabilities to a crate nondestructive assay system. Only simulated passive coincidence data is examined here, although the higher signal rates from active coincidence counting hold more promise for waste management. The active coincidence approach has significantly better sensitivity than the passive and is not significantly perturbed by (alpha,n) contributions. Our study was based primarily on simulated neutron pulse trains derived from the Los Alamos SIM3D software, which were subjected to analysis using the Los Alamos CTEN_FIT and TGS_FIT software. We found significantly improved imaging capability using the coincidence and singles rate data than could be obtained using the singles rate alone.

INTRODUCTION

Standard neutron multiplicity assay algorithms for ^{240}Pu assume a point source of fission neutrons that are detected in a single detector channel. This is consistent with passive neutron assay system designs, which typically have a large number of neutron detectors in an approximately 4-π geometry ganged together so that a single pulse train is observed and the system must be described by a single counting efficiency term. The Pu in real waste, however, is more likely to be distributed throughout the container in some random way. This leads to significant errors when using multiplicity techniques (i.e., "triple" or higher order coincidences) to estimate the effective counting efficiency. Similarly, a simpler coincidence analysis using double coincidence rates to estimate (alpha,n) contributions and an external transmission measurement to estimate matrix losses assumes a uniform distribution of matrix and Pu-240 in the sample, which can lead to large assay errors in interfering matrices.

The use of tomographic emission imaging to improve passive counting results was discussed in ref. [1] for the combined thermal/epithermal neutron (CTEN) passive-active neutron (PAN) assay system. In that study, the net singles rates observed in active neutron counting as a function of the individual detector package and drum angle was

used to generate emission images of the ^{239}Pu in 55 gal. drums. The passive coincidence rate was not used to generate images because the original CAMAC PATRM (pulse arrival time recording module) list-mode coincidence module used in CTEN cannot tag events by detector. With the development of our new PATRM/PCI card, which records the detector number along with the event times, we will be able to generate tagged coincidence data sufficient for tomographic imaging.

In waste assay applications, it is anticipated that the passive coincidence rates attainable at the lower mass range of interest (approx. 1 g low-burn up Pu) will be too low for useful imaging, and in PAN systems the active signal will still be preferred for that purpose. Nevertheless it is instruction to study the passive case, to demonstrate the method and test various design alternatives. It is also simpler to simulate and analyze passive data streams than active data streams. And of course, with dedicated passive counters the option of using the active signal is not available and so the feasibility of passive coincidence imaging is of interest. Passive-only counting applications include high-efficiency passive NDA (nondestructive assay) systems, which have counting efficiencies in the neighborhood of 30-40%, and safeguards applications with modular neutron counters where quantities in excess of 100 g low burn up Pu are of primary interest.

MATHEMATICAL DETAILS

For neutron coincidence imaging we use the "gray barrel" method of Brunson, et al.,[2] to extract the doubles rate d from a neutron pulse train. This is proportional to the rate at which two correlated neutrons are detected within the coincidence time window, which is independent of the (α, n) neutron rate and is proportional to the ^{240}Pu mass, a, in the sample and to the square of the singles counting efficiency, ε. This can be written

(1) $$d = c_d \varepsilon^2 a \quad ,$$

where c_d is a calibration constant. Eqn. (1) describes a single point source and a single detector. We can generalize to n sources of mass a_j ($j = 1, ..., n$) distributed on a grid in space and m detectors viewing those sources from different positions. The entire system is described by the response matrix D, where $D_{ij} \equiv \varepsilon_{ij}$, the efficiency for detecting neutrons emitted from volume element (voxel) j in detector i. In that case we have that

(2) $$d_i = \sum_{j=1}^{n} c_d \varepsilon_{ij}^2 a_j = \sum_{j=1}^{n} D_{ij} a_j \qquad \text{or}$$

$$d = Da$$

in vector notation (d and a are vectors and D is a matrix). An analogous expression for the ordinary (non-coincidence) total neutron rate vector s can be written

(3) $$s_i = \sum_{j=1}^{n} c_s \varepsilon_{ij} a_j = \sum_{j=1}^{n} S_{ij} a_j \qquad \text{or}$$

$$s = Sa$$

where c_s is a calibration constant and the s_i are the rates observed in the i'th detector from the combined sources. The matrices D and S and data vectors d and s are linearly independent and so (2) and (3) can be combined into a single system of equations,

(4) $$r_i = \sum_{j=1}^{n} R_{ij} a_j \qquad \text{or}$$

$$r = Ra \qquad ,$$

where

(5) $$i = 1, 2, ..., 2m$$

$$r_i = d_i \text{ and } R_{ij} = D_{ij} \text{ when } 1 \le i \le m,$$

$$\text{or } r_i = s_{i'} \text{ and } R_{ij} = S_{i'j} \text{ when } m < i \le 2m \ (i' = i - m) .$$

With good quality data and a optimal detector arrangement, the system of equations in (4) can be solved to produce significantly better mass images a than either (2) or (3) alone. Intuitively, one can think of the non-coincidence formulation (3) as being "far-sighted," while the coincidence formulation is "near-sighted." That is, the coincidence rates d fall off much faster with distance than do the non-coincidence rates, s.

We have used the term "detectors" loosely so far to mean either different individual detectors counting at the same time or the same detector used in a different position at different times (a more exact term for this would be "views"). In the case where we have m' $(1 < m' \le m)$ detectors counting simultaneously in a tagged list mode module such as the PATRM/PCI, we can extract doubles rates between pairs of the detectors to further to augment the problem. This can be done extracting the coincidence rate $d(i_1+i_2)$ for the summed detectors i_1 and i_2 by merging their pulse trains and performing the usual coincidence analysis. This leads to the expression for summed detectors

(6) $$d(i_1 + i_2) = \sum_{j=1}^{n} c_d (\varepsilon_{i1,j} + \varepsilon_{i2,j})^2 a_j$$

$$= \sum_{j=1}^{n} c_d \varepsilon_{i1,j}^2 a_j + \sum_{j=1}^{n} c_d \varepsilon_{i2,j}^2 a_j + \sum_{j=1}^{n} 2 c_d \varepsilon_{i1,j} \varepsilon_{i2,j} a_j$$

$$= d_{i1} + d_{i2} + 2d_{(i1,i2)}$$

where $d_{(i1,i2)}$ is the rate at which at neutrons correlated with a trigger neutron in detector i_1 are detected within the coincidence time window in detector i_2. Within statistical error,

$d_{(i1,i2)} = d_{(i2,i1)}$, the rate for detection of detector i_1 neutrons correlated with i_2 triggers. The d_{i1} and d_{i2} terms in (6) are already included in our response matrix, so it is desirable to replace (6) with just the cross term $d_{(i1,i2)}$, and write

(7)
$$d_{(i1,i2)} = \sum_{j=1}^{n} c_d \varepsilon_{i1,j} \varepsilon_{i2,j} a_j \; .$$

The combined doubles and non-coincidence response matrix R can be further expanded by adding rows for the cross terms for a set of suitable detector pairs $\{i_k, i_l\}$. With m' detectors available for pairing, the number of possible pairs is given by

(8)
$$\binom{m'}{2} = \frac{m'(m'-1)}{2} \qquad .$$

We will model the use of pairs in an $m' = 32$-detector B-25 box assay system, in which the box is rotated 180° during the assay, yielding $m = 64$ tomographic views each for the doubles and non-coincidence matrices. Without the cross terms the R matrix models 128 tomographic views, or measurements. Adding all possible pair cross terms would expand the number of views to 624 - almost a factor of 5 increase in the amount of data with which to solve the problem. However, in a counter large enough to accommodate our example case, which is a B-25 box (4' × 4' × 6'), the coincidence rates between most pairs will be too small to be useful. Coincidence rates comparable to those for detector self-coincidence (the squared terms) are only likely between neighboring detector pairs. For the simulated detector geometry described here we used only 79 pairs, which gives a total of 286 views for the two box positions.

Tabulating double coincidence rates between three or more detectors at once does not add new information to the problem. Since only two neutrons are involved, the higher order cross terms are all expressible in terms of paired and single detector terms. For example, for three detectors eqn. (6) becomes

(9)
$$d(i_1 + i_2 + i_3) = \sum_{j=1}^{n} c_d (\varepsilon_{i1,j} + \varepsilon_{i2,j} + \varepsilon_{i3,j})^2 a_j$$

$$= d_{i1} + d_{i2} + d_{i3} + 2d_{(i1,i2)} + 2d_{(i1,i3)} + 2d_{(i2,i3)} \quad .$$

Restricting ourselves to doubles rates in a single detector and between two detectors at a time, and non-coincidence (or singles) rates, we obtain our final neutron coincidence response matrix F by augmenting R with cross terms, i.e.,

(10)
$$f_i = \sum_{j=1}^{n} F_{ij} a_j \qquad \text{or}$$

$$\boldsymbol{f} = F\boldsymbol{a} \qquad ,$$

where $\qquad i = 1, 2, ..., 2m + m_{pair}$

$$f_i = r_i, \quad F_{ij} = R_{ij} \quad \text{if} \quad i \leq 2m \quad ,$$

$$f_i = d_{il,ik} + d_{ik,il} \,, \quad F_{ij} = 2c_d \, \varepsilon_{il,j} \, \varepsilon_{ik,j} \quad \text{otherwise .}$$

The indices i_l and i_k are from a restricted set of pairs (not necessarily all possible pairs) that are m_{pair} in number. Note that we are using the sum of the complementary cross terms, $d_{il,ik} + d_{ik,il}$, rather than one or the other, to obtain better counting statistics. As mentioned before, the two terms are equal within counting error.

The three ways to measure the cross term $2d_{(il,ik)}$ are the cross sorting method, the difference method, and an average of the two. In the cross sorting method, a detector-tagged pulse train is analyzed by the usual gray barrel method, with the difference that in forming signal-triggered histograms only triggers from detector i_l are recognized, and only coincidences with detector i_k are tabulated. The Feynman (random-triggered) histogram does not tally pulses from the trigger detector i_l . The coincidence rate determined by this method is the same within counting error as the $2d_{(ik,il)}$ value obtained by switching the detector roles, so a better value can generally be obtained by using the sum $d_{(il,ik)} + d_{(ik,il)},$ which is the approach we have used here.

In the difference method the cross term is found by rearranging eqn. (6) to obtain

(11) $\qquad 2d_{(i1,i2)} = d(i_1 + i_2) - d_{i1} - d_{i2} \quad .$

This has the advantage that ordinary coincidence sorting algorithms can be used, without detector tagging. In particular, d_{il} and d_{ik} can be obtained from shift registers dedicated to those detectors, while $d(i_l+i_k)$ is measured with a third shift register counting the combined (OR'd) signal.

We can judge which method gives the lowest relative error using data collected on the CTEN (combined thermal epithermal neutron) system at the Los Alamos RANT (Radioassay and Nondestructive Testing) facility. The CTEN separately collects and saves non-tagged list mode data using an older model PATRM module for the sums of the Cd-shielded and unshielded ^{3}He detectors, with counting efficiencies of 11.8% and 5.4%. The CTEN_FIT software, used to analyze CTEN data, can cross sort between the two pulse trains and can also merge the two pulse trains (they are synchronized to the same clock pulse). Figure 1 compares the relative std. dev. (RSD) for the cross terms calculated by the three methods for replicate assays of a series of 8 PuO standards or combinations of standards (totaling 3 ,10, 25, 50, 100, 125, 150, 175, and 200 g of ^{239}Pu). An average of 7.5 assays per case were performed. For this data, the figure shows that the cross sorting and difference methods give nearly the same error, with average RSDs of 4.6% and 4.5%, respectively. The two results appear to be at least partially independent, as their average has a slightly lower average RSD of 3.5%.
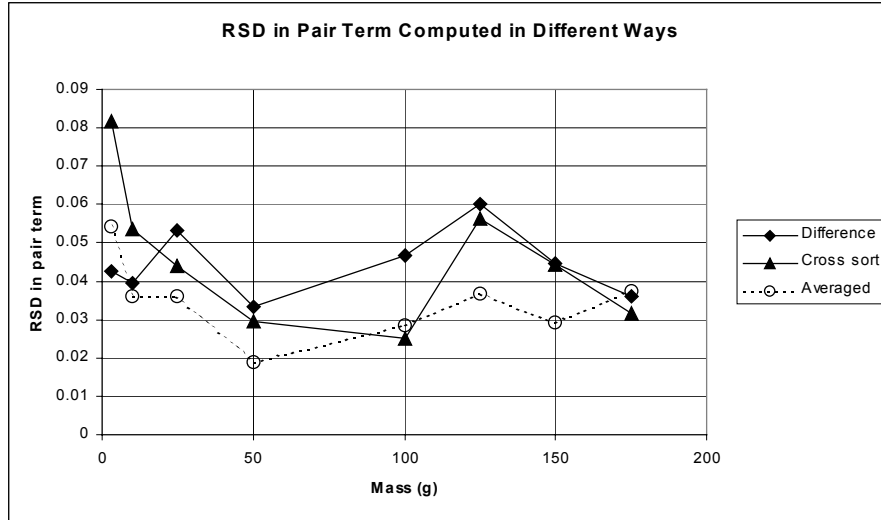
RSD in Pair Term Computed in Different Ways

Figure 1. Average rel. stdev. (RSD) in cross terms computed by the difference method, the cross sorting method, and their average, as a function of the ^{239}Pu mass in PuO_2 standards counted passively on the CTEN instrument. The cross terms are from the shielded versus the bare ^3He detector packages.

DETECTOR PLACEMENT

We modeled two B-25 box counting systems, both with 40% neutron counting efficiencies (for normal, non-coincidence counting). One system uses 32 detectors placed in an alternating criss-cross pattern so that if the crate is rotated by 180° every face will by counted by two arrays of ^3He detector tubes oriented at right angles. The detector tube spacing of 1 ft matches the desired image resolution of 1 ft^3 voxels (i.e., a $4 \times 4 \times 6$ grid of $n = 96$ voxels). With only 64 views available in singles-only (non-coincidence) counting, this is an underdetermined system and eqn. (3) cannot be solved without the addition of the coincidence terms. Generally, using a natural detector spacing equal to the voxel size will always result in an underdetermined system of equations with a box counter. To create more views, we have modeled a 56-detector system in which the detector spacing is reduced to 0.5 ft by inserting additional detector tubes halfway between those in the 32-detector system. In practice, a 40% efficient B-25 box counter would have many more detector tubes than are used here, so our 32- and 56-detector systems represent different ways to gang adjacent detector tubes into a single package. The total efficiency therefore is the same for both cases, while the efficiency per detector is correspondingly less in the 56-detector design. Figure 2 shows the detector placement for both the 32- and 56-detector systems.

MODELING METHODS

We used the TGS_FIT 2.0 image reconstruction software to perform all emission imaging, using the non-negative least squares (NNLS) algorithm. The NNLS algorithm

gives an exact least-squares fit to the data subject to the constraint that all image voxels must be nonnegative. TGS_FIT offers numerous options for simulation of data, including the addition of Poisson noise (see, for example, ref. [3], which was presented in another session at this conference). However, the noise in the doubles coincidence rates d_i is not adequately represented by simple Poisson error and is correlated with singles and other coincidence rate errors in a complex way. To obtain realistic noise levels, we simulated our neutron coincidence data using the Los Alamos-developed SIM3D software to model actual pulse trains of neutrons.

The undocumented SIM3D program takes as input the singles efficiency matrix S (of eqn. (3)), the true ^{240}Pu mass vector a, the ratio of total to fission neutrons, the detector dieaway time, and the count time to randomly generate separate neutron pulse trains for the total system (all detectors combined) and for each single detector. These pulse trains were then analyzed using the CTEN_FIT databasing and analysis program. As mentioned above, CTEN_FIT allows two separate but synchronized pulse trains to be analyzed both in sum mode (as a merged stream) and by cross-sorting between the two trains, as described above. Using a list of adjacent detector pairs, the SIM3D program generated paired sets of the single-detector pulse train list files, which were then analyzed in CTEN_FIT to obtain the cross terms. The coincidence data modeled in this way has the correct error distribution, which can be described loosely as very good counting statistics for the singles rates (i.e., non-coincidence rates) and relatively poor counting statistics for the coincidence rates.

We have modeled several source distributions. One of the most difficult to image with a crate counter geometry is illustrated below in figure (3a). This distribution has only two voxels, each with 0.5 g of ^{240}Pu. They are located vertically in adjacent middle layers 2 and 3, and horizontally at opposite corners of the 4-voxel layer center groups. The two voxels thus touch at one corner. This is the only mass distribution reported on here.

Figure 2. Schematic representation of the detector placement in the 32- and 56-detector B-25 box counter designs. The dashed lines show the additional 24 detectors in the 56-detector case. Note that each tube (possibly) represents more than one tube ganged together, and that the two schemes are interpreted as different ways to group a much larger number of tubes. Therefore both designs have the same overall efficiency.
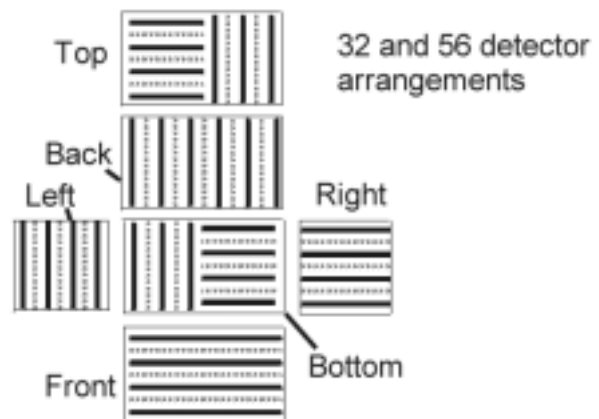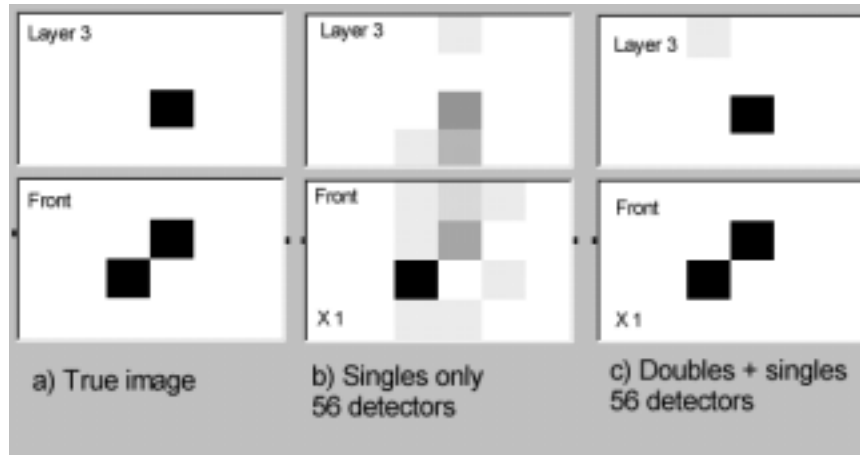
Figure 3. Reconstructions of a two-voxel image from a 5000-s count of a total of 1 g ^{240}Pu. The degree of darkness is proportional to the imaged ^{240}Pu mass. For each of the three image pairs, the bottom image is the summed front view (radiographic view) and the top is a tomographic slice view of the third layer (see figure 4 for the horizontal position of the layer 2 voxel). a) The true image, b) the image reconstructed from singles (non-coincidence) counts only, and c) the improved image reconstructed from combined singles and doubles rates.
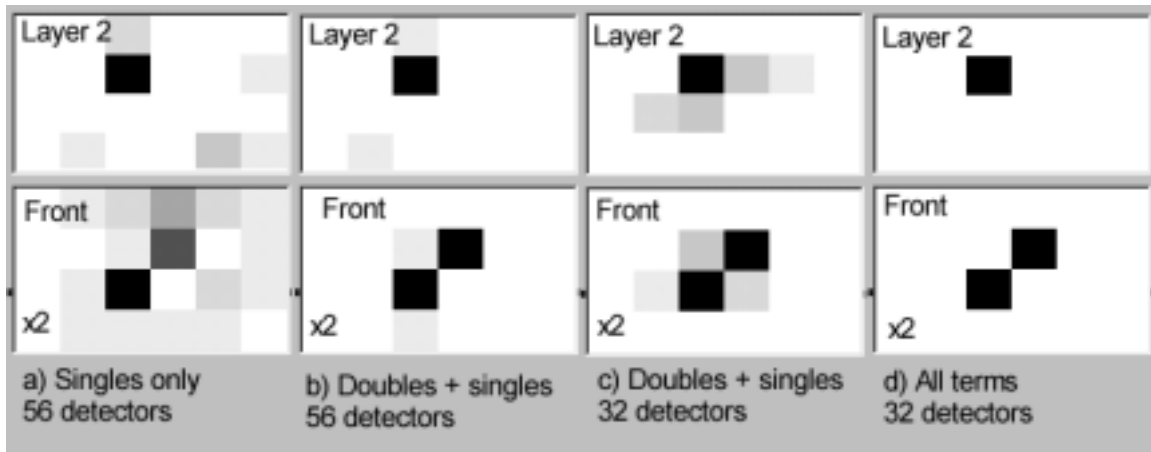

Figure 4. More reconstructions of the two-voxel image in figure3, shown at twice the mass display range as in 3. Layer 2 is shown in this case. a) The image from 56-detector singles (non-coincidence) counts only (same as 3b), b) the image from 56-detector combined singles and doubles rates (same as 3c), c) the image from 32-detector combined singles and doubles rates, and d) the image from 32-detector combined singles, doubles, and paired detector (cross term) rates . The image in (d) is indistinguishable on this scale from the true image.

RESULTS AND DISCUSSION

Fig. 3a-b shows the effect on imaging capability of adding the doubles coincidence rates to the singles-only problem. Fig. 3a shows the true distribution of ^{240}Pu mass; fig 3b shows the image produced using singles rates only from a 5000-s count, as in eqn. (3); and fig 3c shows the image produced from the same data using both the singles and doubles rates, as in eqn (4). Clearly, the image quality was significantly improved by the addition of the doubles coincidence rates.

Fig. 4a and 4b show the same images as in fig. 3b and 3c, this time with a different layer slice view shown and with an image intensity twice the full range to more clearly show errors in the reconstructions. Figure 4 illustrates our primary conclusion, which is that adding (self-coincidence) doubles rates for single detectors greatly improves imaging ability over the use of singles (non-coincidence) counting alone, and that adding cross-coincidence rates between adjacent pairs of detectors further improves imaging power. Note in particular that the use of all coincidences in fig 4d gives a significantly better image with 32 detectors than when using the doubles and singles counting only with 56 detectors.

We conclude that, in general, the use of coincidence data can significantly enhance image reconstructions compared to singles rates only. Having just recently developed the software tools needed for studying this problem, we have only examined a few cases so far and it would be premature to make detailed performance predictions for PAN or passive-only counters similar to those currently fielded, with or without the criss-cross detector arrangement shown in fig. 2. Nor can we make predictions at this point for other types of systems, such as applications to barrel counters or mobile pods for safeguards measurements. Nevertheless, we are optimistic that the method can be applied in waste management scenarios to active neutron counting and in safeguards scenarios to passive counting.

REFERENCES

1) R.Estep, S. Melton, and D. Miko, "Methods for Reducing Bias in Combined Thermal/Epithermal Neutron (CTEN) Assays of Heterogeneous Waste," 6th NDA Waste Characterization Conference, Salt Lake City, Utah, Nov. 17-19, 1998.

2) G. Brunson and N.J. Nicholas, "Shift-Register Neutron-Coincidence Counting and the Gray Barrel Problem," Los Alamos Rept. LA-12414-MS (Oct. 1992).

3) R. Estep, R. Brandenburg, and J. Wachter, "Low-Mass Bias Issues in Tomographic Gamma Scanning (TGS)," published in this conference proceedings.